Available online at www.sciencedirect.com
ScienceDirect
Procedia Materials Science 8 (2015) 180 – 189
Procedia Materials Science
www.elsevier.com/locate/procedia

International Congress of Science and Technology of Metallurgy and Materials, SAM - CONAMET 2013

Sintering and Microstrusture of Al_2O_3 and Al_2O_3-ZrO_2 Ceramics

Heidy L. CALAMBÁS PULGARÍN* and María P. ALBANO

Centro de Tecnología de Recursos Minerales y Cerámica (CETMIC), M. B. Gonnet, Provincia de Buenos Aires, Argentina.

Abstract

Alumina powder and two commercial 3 mol% yttria-partially stabilized zirconia powders–0.3 wt% Al_2O_3-doped (Al-Y-PSZ) and without Al_2O_3 (Y-PSZ)–were used to produce alumina-zirconia (Al_2O_3-ZrO_2) slip cast composites. The influence of the substitution of Al_2O_3 by 50 vol% of the different zirconia powders on the sintering kinetic at the intermediate stage was investigated. In addition, the microstructure of Al_2O_3 and the different composites at temperatures in the range of 1100-1600°C was studied and related to the sample hardness. An increase in the sintering rate was observed when 50 vol% Y-PSZ was substituted by 50 vol% Al-Y-PSZ. 50 vol% zirconia was effective to reduce the rate of Al_2O_3 grain growth in the final sintering stage. For 50 vol% Al-Y-PSZ a smaller ZrO_2 grain size distribution compared with 50 vol% Y-PSZ could be achieved. As the average Al_2O_3 grain size of the sintered samples became greater than about 1 μm a markedly decrease in the hardness was found; this occurred at temperatures higher than 1400°C, since de composites with 50 vol% zirconia reduced the rate of Al_2O_3 grain growth a decrease in hardness up to 1600°C was not observed.

Selection and peer-review under responsibility of the scientific committee of SAM - CONAMET 2013

Keywords: Al_2O_3 – ZrO_2, sintering behaviour, microstructure, hardness.

1. Introduction

The alumina (Al_2O_3) and alumina-zirconia (Al_2O_3-ZrO_2) ceramics are suitable for a variety of high demanding applications including dental screws, cutting blades, electrosurgical insulators, valve seals, body armor, pump components, oxygen sensors, dies, and prosthesis components such as hip joints, by Y. Shin et al. (1999), due to

* Tel.: +54 0221 484 0247 int 107
E-mail address: hlcalambas@cetmic.unlp.edu.ar

Selection and peer-review under responsibility of the scientific committee of SAM - CONAMET 2013
doi:10.1016/j.mspro.2015.04.062

their attractive properties, including high-temperature mechanical strength, good thermal shock resistance, wear and oxidation resistance, low thermal conductivity, and the close match between their thermal expansion coefficients and those of metals, by J. Wan et al. (1989) and S. Olhero et al. (2009).

Colloidal processing methods allow to get green bodies with good microstructural homogeneity. Sintering of them represents great importance because it gives the microstructure and final properties of ceramics.

Sintering models can be used to determine the diffusion mechanisms and activation energy. The sintering kinetics was studied measuring the contraction of the material as a function of time at different constant temperatures.

In this work, the influence of the substitution of Al_2O_3 either by 50 vol% of the different zirconia powders on the sintering kinetic at the intermediate stage was investigated. In addition, the microstructure of Al_2O_3 and the different composites at temperatures in the range of 1100-1600°C was studied and related to the sample hardness.

2. Experimental Procedure

2.1. Raw materials and powder processing

In this study, alumina powder (A16 SG, Alcoa Chemicals, USA, d_{50}=0.40 μm), and 3 mol% yttria-partially stabilized zirconia with 0.3 wt% Al_2O_3 (Saint-Gobain ZirPro, d_{50}=0.23 μm) and without Al_2O_3 (Saint-Gobain ZirPro, d_{50}=0.64 μm) powders were used. A commercial ammonium polyacrylate solution (NH_4PA) (Duramax D 3500, Rohm & Haas) was used as deflocculant. 48 vol% aqueous suspensions with different compositions (100 vol% Al_2O_3, and 50 vol% Al_2O_3 - 50 vol% zirconia powders respects to the total solid loading) with the optimum NH_4PA concentration (0.32, 0.52 and 0.11 wt% of Al_2O_3, 50vol% Al_2O_3 – 50vol% Al-YPZ and 50vol% Al_2O_3 – 50vol% YPZ, respectively) were prepared using ultrasonic disruption; the pH was manually adjusted to 9. Slips were cast into rectangular shape plaster molds (12 x 10 x 9 mm); the consolidated samples were dried 100 °C. The green samples were sintered in air at 1100-1600 °C for 2 h (heating rate 5 °C/min).

2.2 Characterization techniques

The specific surface area (S_g) of the powders was measured using a Micromeritics Accusorb sorptometer.

The density of the green compacts was determined by the Archimedes method using mercury displacement. The bulk density of the sintered samples was determined by water immersion (ASTM C20-00). The sintered samples were polished with a series of diamond pastes down to 1/4 μm. The Vickers hardness (Hv) was carried out using a diamond indenter (Buehler hardness tester) at a load of 3 kgf with an indentation period of 30 s. Ten Hv measurements were used to obtain an average value. The alumina and zirconia grain sizes were measured using SEM micrographs (JEOL, JSM-6360) of polished and thermally etched surfaces.

The isothermal shrinkage measurements were performed as follows: the temperature of the specimens was first increased at a constant rate of 10°C/min to 800°C, held at that temperature for 10 min, and subsequently increased rapidly at about 50°C/min to the set temperature, which was in the range of 1150-1400°C. The length shrinkage was measured as a function of time at the constant set temperature for 2h. When the time reached 2h, the specimens were cooled.

3. Results And Discussion

3.1 Densification and grain growth

The specific surface area (S_g) values for Al_2O_3, Y-PSZ and Al-Y-PSZ powders were 8.74, 7.84 and 12.25 m^2/g, respectively.

In a previous work by Heidy L. Calambás Pulgarín et al. (2012), the present authors correlated the density of green samples with the rheological behavior of the suspensions. We noted that the suspensions of Al_2O_3 with Y-PSZ had the lowest of viscosity values and produced denser particle packing by slip casting.

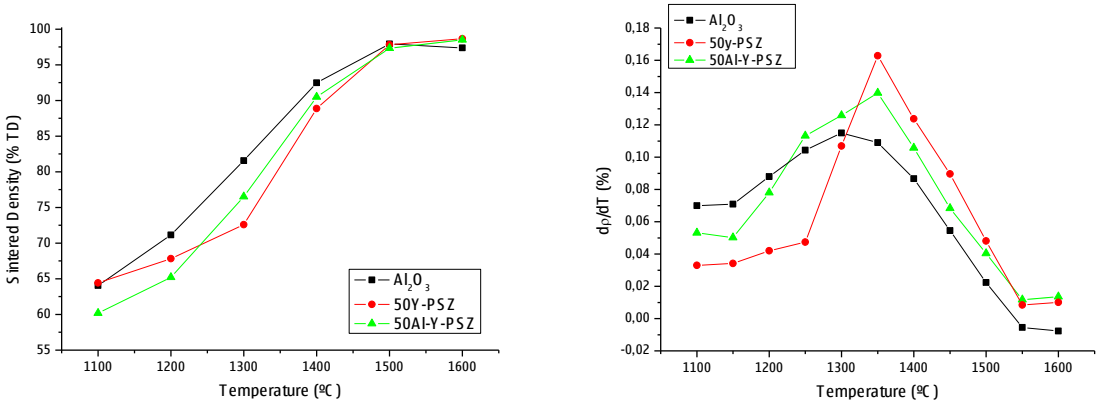

(a) (b)

Fig. 1 (a) Relative sintered density versus sintering temperature curves (b) Derivatives of sintered density with respect to temperature for Al_2O_3, 50Al-YPZ and 50YPZ.

Figures 1a and 1b show the change in the relative sintered density (% theoretical density) and the derivatives of sintered density with respect to temperature (dρ/dT), versus the sintering temperature. At the intermediate sintering stage (1200-1400°C), the densification rate of Al_2O_3 was higher than that of the composites Al_2O_3-ZrO_2. The curves in Figure 1b showed a maximum, a higher peak temperature was found for the composites relative to that of Al_2O_3. (1300ºC for Al_2O_3 and 1400ºC for the composites) Differences between the composites were observed: 50 vol% Al-Y-PSZ (50Al-Y-PSZ) began to sinter at lower temperatures with respect to the composite with 50 vol% (50Y-PSZ), and higher sintered densities at 1250-1400 °C could be achieved.

The isothermal shrinkage behaviour of Al_2O_3 and Al_2O_3-ZrO_2 compacts was examined. Both values of the activation energy and the frequency-factor term in the applied sintering-rate equations were estimated from the isothermal shrinkage curves. The sintering-rate equation for isothermal shrinkage is given by K. Matsui et al. (2007):

$$\frac{\Delta L}{L_o} = \left(\frac{K\gamma\Omega D}{kTa^p}\right)^n t^n \tag{1}$$

where $\Delta L (= L_0 - L)$ is the change in the length of the specimen, L_0 the initial length, K a numerical constant, γ the surface energy, Ω the atomic volume, D the diffusion coefficient, t the time, T the absolute temperature, k the Boltzmann's constant, a the spherical particle radius, and the parameters n and p the order depending on the diffusion mechanism. The values of p for grain-boundary diffusion (GBD) and volume diffusion (VD) are p=4 and p=3, respectively. Equation 1 is applicable to the fractional shrinkage of < 4, which satisfy the intermediate sintering stage.

On taking logarithms, the following equation is obtained:

$$log\frac{\Delta L}{L_o} = nlog\left(\frac{K\gamma\Omega D}{kTa^p}\right) + nlog(t) \tag{2}$$

Moriyoshi et al. (1970) have reported that the log ($\Delta L/L_0$) vs log t plot of Eq. (2) does not show linear relationship when the grain growth proceeds simultaneously. Thus, the isothermal sintering experiments should be

analyzed carefully since the log-log plot of the shrinkage curve depends not only on the diffusion coefficient but also on the grain size.

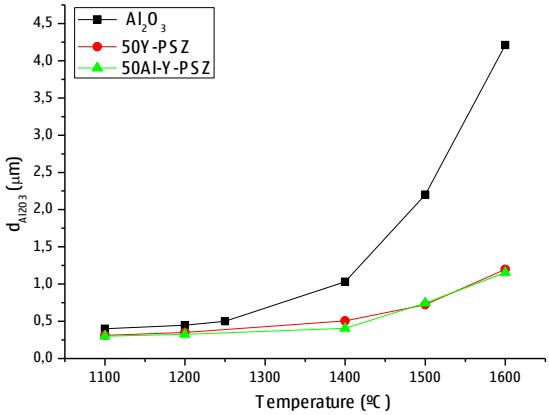

Fig. 2. Mean grain diameters (d_{50}) of Al_2O_3 and Al_2O_3-ZrO_2 composites as a function of the sintering temperature in the different composites

Therefore, the mean grain diameters of Al_2O_3 in the different compacts were measured as a function of the sintering temperature and are shown in Figure 2.

The Al_2O_3 grain diameter in pure alumina remained nearly constant in the temperature range 1100-1250°C, then a slightly increased in the grain diameter with increasing sintering temperature up to 1400°C was found, followed by a significant increase with further increasing in temperature up to 1600°C. The Al_2O_3 grain diameter in the composites remained virtually unchanged up to 1400°C. No significant differences in the Al_2O_3 grain diameter versus temperature curve between 50Al-Y-PSZ and50Y-PSZ were found.

The significant Al_2O_3 grain growth in pure Al_2O_3 decreased the sintering rate at T>1400 °C (Equation 1) and let to a sintered density (ρ_{sint}) at 1600 °C lower than that observed for the composites Al_2O_3-ZrO_2 (Fig 1a). Similar density values at 1600 °C, 98.48 and 98.65% of the theoretical density, were measured for the composites with Al-Y-PSZ and Y-PSZ, respectively.

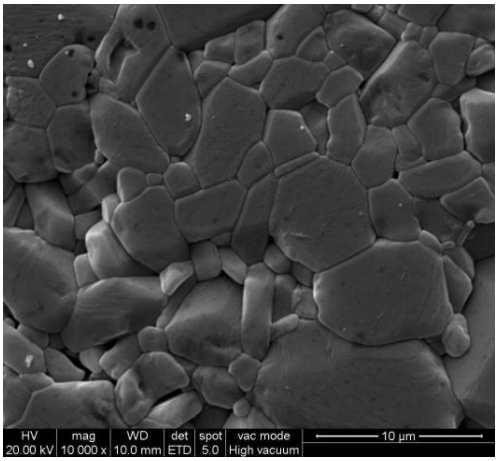

(a)

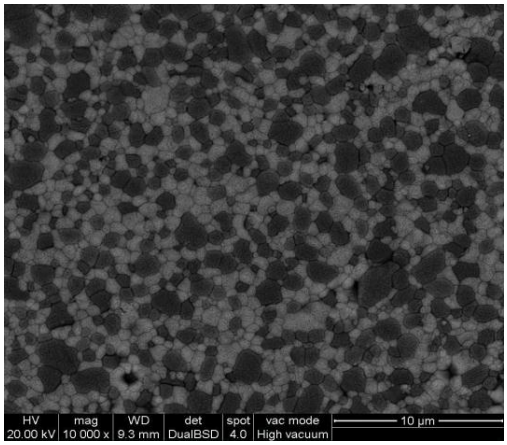

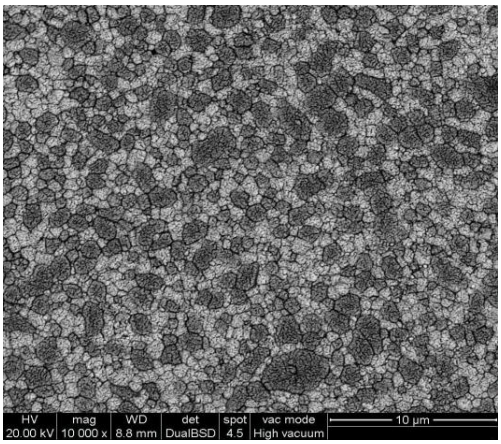

(b) (c)

Fig. 3. SEM micrographs of different samples sintered at 1600°C: (a) Al_2O_3; (b)50Al-Y-PSZ (c) 50Y-PSZ.

Figure 3 shows the microstructure of Al_2O_3, 50Al-Y-PSZ and 50Y-PSZ sintered at 1600 °C. The micrographs (b and c) show ZrO_2 grains (the brighter phase) homogeneously distributed in a fine grain Al_2O_3 matrix (the darker phase). The ZrO_2 grains inhibited the Al_2O_3 grain growth during the final sintering stage (1400-1600°C); thus, the ZrO_2 particles occupied the intergranular boundaries and often the triple points between Al_2O_3 grains. This had the effect of pinning the alumina and prevented grain growth. 50 vol% zirconia was effective inhibiting Al_2O_3 grain growth. For Al_2O_3 the rapid grain growth at 1400-1600°C let to a grain diameter at 1600°C that was 3.5 times greater than the grain diameter obtained for the composites with 50 vol% zirconia (Fig. 2).

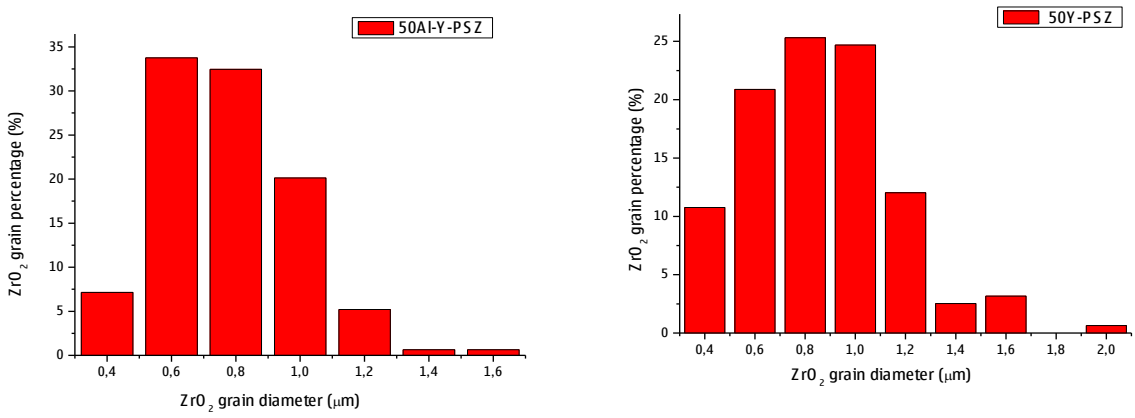

(a) (b)

Fig 4. Grain size distribution ZrO_2 in the different composites sintered at 1600 ° C (a) 50ZPS-dAl and (b) 50ZPS.

Figure 4 presents the ZrO_2 grain size for the different composites at 1600 °C. The 50Al-Y-PSZ curve was slightly shifted to lower diameters with respect to that of 50Y-PSZ. The most frequent grain diameter was 0.6 and 0.8 μm for Al-Y-PSZ and Y-PSZ, respectively. The smaller ZrO_2 grain diameter for 50Al-Y-PSZ with respect to 50Y-PSZ was attributed to the finer Al-Y-PSZ particles relative to those of Y-PSZ.

The sintering temperature at which the Al_2O_3 grains did not change was 1150-1250 °C for Al_2O_3 and 1250-1400 °C for 50Al-Y-PSZ and 50Y-PSZ. These temperature ranges were selected to analyze the isothermal shrinkage curves of each sample.

3.2 Isothermal shrinkage analysis

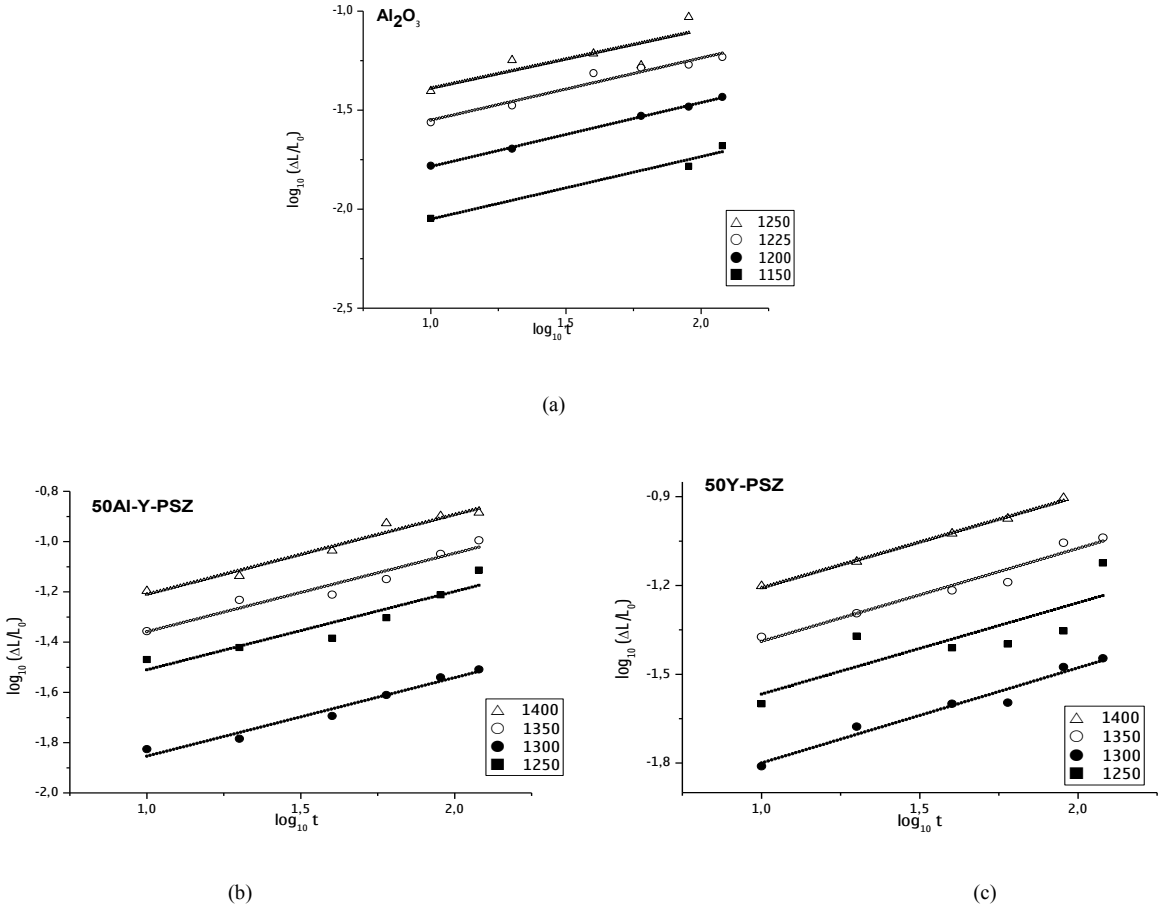

Fig. 5. Logarithm shrinkage - Logarithm time plots of: (a) Al_2O_3, (b) 50Al-Y-PSZ and (c) 50Y-PSZ at four different temperatures.

Figure 5 shows the log-log plots of the isothermal shrinkage versus heating time curves for Al_2O_3, 50Al-Y-PSZ and 50Y-PSZ at four different temperatures. All the log-log plots showed linear relationships and the data satisfactory fitted to a slope of 1/3 (n=1/3, Eq. 2). These results indicated that the sintering rate of Al_2O_3 and the composites was controlled by grain boundary diffusion mechanism (GBD) by K. Matsui et al. (2007). The activation energy and frequency factor term of each specimen were estimated using the values of the constant term in Eq. (2). This constant term corresponded to the intercept of the straight line on the vertical axis in Figure 5 when log t is 0.

Using as $\beta = \frac{K\gamma\Omega D}{Tka^p}$ (Eq. 2) and using the general expression of the diffusion coefficient, $D = D_o\left({}^{-Q}/_{RT}\right)$ the following equation is obtained:

$$\beta T = \beta_0 exp\left({}^{-Q}/_{RT}\right) \quad (3)$$

Where $$\beta_0 = \frac{K\gamma\Omega D_0}{ka^p} \quad (4)$$

On taking natural logarithm in Eq. (3) resulted in :

$$\ln(\beta T) = ln\beta_0 - \frac{Q}{RT} \quad (5)$$

where Q is the activation energy, R the gas constant, and D_0 the preexponential term of the diffusion coefficient.

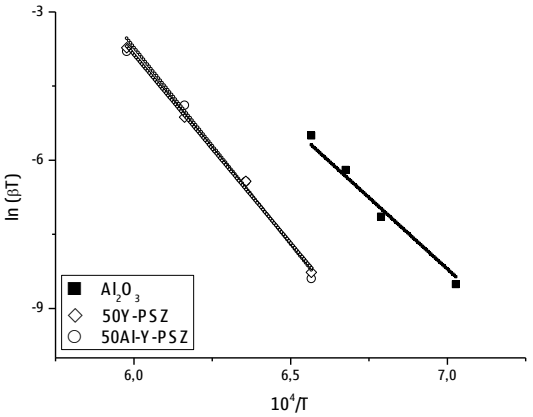

Fig. 6. Arrhenius-type plots of ln(βT) against 1/T for Al_2O_3 50Al-doped Y-PSZ and 50Y-PSZ composites.

Figure 6 shows the Arrhenius-type plots of ln(βT) against 1/T for Al_2O_3 and the 50Al-Y-PSZ and 50Y-PSZ composites. The plots of all specimens showed linear relationships; the Q value of each sample was determined from the slope of the straight line by applying Eq. (5) to the Arrhenius-type plot in Figure 6. The value of β_0 was also determined from the intercept of the straight line on the vertical axis when 1/T=0. The Q and β_0 values of Al_2O_3 and the Al_2O_3-ZrO_2 composites are presented in table 1. The activation energy of GBD in Al_2O_3 was smaller than that of the Al_2O_3- ZrO_2 composites. Thus, the greater sintering rate of Al_2O_3 with respect to that of the composites was attributed to the lower activation energy value (Eqs. 1-5).

Table 1. Activation energy and frequency for the sintering of Al_2O_3 and the composite factor.

Muestra	Energía de Activación (KJ/mol)	Factor de Frecuencia lnβ_0
Al_2O_3	480±20	32
Al_2O_3-ZPS-dAl	690 ±20	50
Al_2O_3-ZPS	670 ±20	41

In the case of alumina-zirconia, our measurements of the activation energy agreed well with the work of Wakai et al. (1989) who obtained the following values for alumina-zirconia (3 mol% yttria): 723 KJ/mol for 50 vol% Al_2O_3 and 681 kJ/mol for 85.7 vol% Al_2O_3. Wang et al. (1991) also reported an activation energy of 730 ± 60 kJ/mol for alumina containing 5 vol% ZrO_2; they correlated the activation energies of alumina and alumina/zirconia with their respective interfacial energies. The alumina/zirconia interface energy was lower than that of alumina/alumina by a factor of 1.5 which was nearly the same as the ratio of the activation energies for boundary diffusion in these two types of interfaces.

Matsui et al. (2007) studied the effect of the specific surface area of different zirconia powders on the initial

sintering stage; they concluded that the increase in the specific surface area of fine zirconia powders enhanced the shrinkage rate because of an increase in β_0. In the present work, the specific surface area of the Al-Y-PSZ particles was markedly higher than that of Al_2O_3 or Y-PSZ, consequently a higher β_0 value could be expected when a large amount of Al_2O_3 or Y-PSZ was substituted by Al-Y-PSZ. Therefore, the increase in the β_0 value with the substitution of 50 vol% Y-PSZ by Al-Y-PSZ was a consequence to the increase in the specific surface area of the powders, resulting in an increasing sintering rate.

Matsui et al. (2008) also investigated the effect of Al_2O_3 concentration on the sintering of fine ZrO_2 powders; they demonstrated that an increase in the Al_2O_3 content from 0 to 1 wt% enhanced the densification rate because of the increase in both n with the change of diffusion mechanism from grain boundary to volume diffusion and β_0 (Eq. 7). This enhanced sintering mechanism was reasonably interpreted by the segregated dissolution of Al_2O_3 at ZrO_2 grain boundaries. Therefore, the higher sintering rate at the intermediate stage of 50Al-Y-PSZ relative to 50Y-PSZ could be attributed to the increase in the specific surface area of the powders together with the enhanced densification produced by the Al_2O_3 doping.

3.3 Sample hardness

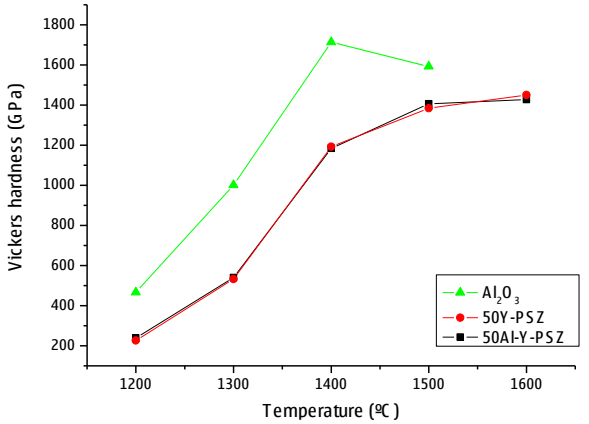

Fig. 7. Vickers hardness versus the sintering temperature for Al_2O_3 and 50Al-Y-PSZ and 50Y-PSZ composites.

Figure 7 shows the vickers hardness (H_v) versus the sintering temperature for Al_2O_3 and the Al_2O_3-ZrO_2 composites. For all the samples the hardness increased with increasing sintering temperature from 1300 to 1400°C as a consequence of the increase in the relative sintered density (Fig. 1a). Thus, at 1300-1400°C the higher relative sintered density of Al_2O_3 resulted in higher H_v values. Although the sintered density of Al_2O_3 increased with further increasing in temperature from 1400 to 1500 °C a maximum hardness was found at 1400°C. On the contrary, 50Al-Y-PSZ and 50Y-PSZ did not show a maximum instead the H_v value increased up to 1600°C.

This behaviour was related with the Al_2O_3 grain growth versus temperature curves shown in Fig. 2 When the Al_2O_3 average grain diameter increased over about 1 µm a markedly decrease in the H_v values was found; this occurred at T> 1400°C for Al_2O_3. According to Rice et al (1994) the generally accepted trend was that H_v increased with decreasing the grain size (G) (e.g., $H_v \alpha G^{-1/2}$) at finer G. For their alumina specimens, Krell et al. (1995) attributed the increase in hardness with decreasing grain size to a reduction in dislocation mobility with decreasing grain size.

In this work, we reported a decrease in the H_v values when the Al_2O_3 became greater than about 1 µm, this occurred at T> 1400°C for Al_2O_3. Since 50 vol% ZrO_2 reduced the rate of Al_2O_3 grain growth (Fig. 2), the Al_2O_3 average grain diameter remained ≤ 1 µm up to 1600 °C and consequently a decrease in H_v was not observed (Fig. 7). 50Al-Y-PSZ and 50Y-PSZ exhibited nearly the same H_v-T dependence in the whole range of temperatures studied. The H_v value for Al_2O_3 at 1400 °C was markedly higher than that of 50Al-Y-PSZ and 50Y-PSZ at 1600 °C; since

alumina is harder than ZrO_2 by A. H. De Aza (1995), these differences in the H_v values could be attributed to the greater substitution of Al_2O_3 by ZrO_2 in the composites.

4. Conclusions

Two commercial 3 mol% yttria-partially stabilized zirconia powders, 0.3 wt% Al_2O_3-doped (Al-Y-PSZ) and without Al_2O_3 (Y-PSZ), were used to produce alumina-zirconia (Al_2O_3-ZrO_2) slip cast composites. The influence of the substitution of Al_2O_3 either by 50 vol% Al-Y-PSZ or 50 vol% Y-PSZ on the sintering kinetic at the intermediate stage was investigated. In addition, the microstructure of Al_2O_3 and the different composites at temperatures in the range of 1100-1600 °C was studied and related to the sample hardness.

The intermediate sintering stage of both alumina and the composites was controlled by a grain-boundary diffusion mechanism. The densification rate of Al_2O_3-ZrO_2 was lower than that of Al_2O_3 as a consequence of the increase in the activation energy of sintering in the presence of zirconia. An increase in the sintering rate was observed when 50 vol% Y-PSZ was substituted by 50 vol% Al-Y-PSZ. This behaviour could be attributed to the increase in the specific surface area of the Al-Y-PSZ powder together with the enhanced densification produced by the Al_2O_3 doping. For 50 vol% Al-Y-PSZ a smaller ZrO_2 grain size distribution compared with 50 vol% Y-PSZ could be achieved.

As the average Al_2O_3 grain size of the sintered samples became greater than about 1 μm a markedly decrease in the hardness was found; this occurred at temperatures higher than 1400°C for Al_2O_3. Since 50 vol% 50Al-Y-PSZ and 50 vol% Y-PSZ reduced the rate of Al_2O_3 grain growth a decrease in hardness up to 1600 °C was not observed.

References

A. H. De Aza, J.Chevalier, G. Fantozzi, M. Schehl and R. Torrecillas, 2002. Crack growth resistance of alumina, zirconia and zirconia toughened alumina ceramics for joint prostheses. Biomaterials. 23, 937-945.

A. Krell and P. Blank, 1995. Grain size dependence of hardness in dense submicrometer alumina. J. Am. Ceram. Soc. 78, 1118-1120.

F. Wakai, Y. Kodama, S. Sakorguchi, M. Murayama, H. Kato and T. Nagone, 1989. In Proceedings of the MRS International Meeting on Superplasticity. Materials Research Society, Pittsburgh, PA. 7, 259.

Heidy L. Calambás Pulgarin, Liliana B. Garrido, María P. Albano, 2012. Rheological properties of aqueous alumina–alumina-doped Y-PSZ suspensions. Ceramics International. 38, 1843–1849

J. Wang, R. Stevens, 1989. Review zirconia –toughened alumina (ZTA) ceramics. J. Mater. Sci. 24, 3421-3440.

J. Wang and R. Raj, 1991. Activation energy for the sintering of two-phase alumina/zirconia ceramics. J. Am. Ceram. Soc. 74, 1959-1963.

K. Matsui, A. Matsumoto, M. Uehara, N. Enomoto and J. Hojo, 2007. Sintering kinetics at isothermal shrinkage. Effect of specific surface area on the initial sintering stage of fine zirconia powder. J. Am. Ceram. Soc. 90, 44-49.

K. Matsui, T. Yamakawa, M. Uehara, N. Enomoto and J. Hojo, 2008. Mechanism of alumina-enhanced sintering of fine zirconia powder: influence of alumina concentration on the initial stage sintering. J. Am. Ceram. Soc. 91, 1888-1897.

Moriyoshi and W. Komatsu, 1970. Kinetics of initial sintering with grain growth. J. Am. Ceram. Soc. 53, 671-675.

R. W. Rice, C. C. Wu and F. Borchelt, 1994. Hardness-grain-size relations in ceramics. J. Am. Ceram. Soc. 77, 2539-2553.

S. Olhero, I. Ganesh, P. Torres, F. Alves, J. M. F. Ferreira, 2009. Aqueous colloidal processing of ZTA composites. J. Am. Ceram. Soc. 92, 9-16.

Y. Shin, Y. Rhee, S. Kang, 1999. Experimental evaluation of toughening mechanism in alumina-zirconia composites. J. Am- Ceram- Soc. 82, 1229-1232.